On the capability of the Thick Level Set (TLS) damage model to fit experimental data of size and shape effects

Andrés Parrilla Gómez, Nicolas Moes, Claude Stolz, David Grégoire, Gilles Pijaudier-Cabot

Accepted manuscript in Engineering Fracture Mechanics. DOI: 10.1016/j.engfracmech.2017.07.014
The final publication is available at: https://dx.doi.org/10.1016/j.engfracmech.2017.07.014

On the capability of the Thick Level Set (TLS) damage model to fit experimental data of size and shape effects

A. Parrilla Gómez[a,*], N. Moës[a], C. Stolz[a,b], D. Grégoire[c], G. Pijaudier-Cabot[c]

[a] *GeM, UMR CNRS 6183, École Centrale de Nantes, 1 rue de la Noë, 44321 Nantes, France*
[b] *IMSIA, UMR CNRS 9219, EdF, Av. Charles de Gaulle, 92141 Clamart, France*
[c] *LFC-R UMR5150, Université de Pau et des Pays de l'Adour, Allée du Parc Montaury, F64600 Anglet, France*

Abstract

Size and shape effects are important issues in predicting the global behavior of concrete structures. Small-scale tests performed in laboratory to determine the material properties are not enough to simulate large-scale structures. As no full consensus exists on a universal size and shape effects law that could allow to extrapolate small-scale results to large-scale simulations [1], efforts are done to find models able to fit size and shape effects from experimental data. Recently, three models have been compared to two complete experimental campaigns concerning size and shape effects [2, 3]: a lattice model [4], the nonlocal integral damage model [2] and the cohesive zone one [5]. Only the lattice and the cohesive ones were able to properly recover size and shape effects. However, both present main disadvantages: lattice models' computational cost is too high for large-scale structures and cohesive models difficultly deal with crack initiation and complex crack paths such as branching and coalescence. In [6], a level set based regularization for damage models called Thick Level Set (TLS) was presented. In this paper, the capability of this model to represent size and shape effects for two recently published experimental campaigns is studied.

Keywords: damage, TLS, concrete, experimental fit, size effect, shape effect

1. Size effect and shape effect analysis

Since the seventies, it is well known that there exists a so-called size effect in global response of concrete notched beams of different sizes [7]: the apparent critical energy release rate depends on the size of the structure. Later, it was found that a similar size effect exists for unnotched beams. These two size effects are called type I (unnotched structures) and II (notched ones). Having two different laws depending on the existence and the depth of a notch reveals a shape effect. In fact, the transition between size effect of type I and II corresponds to the proximity of the location of damage initiation and the boundary of the structure: in an unnotched beam, damage initiates on the boundary of the domain while in a deeply notched one, it appears at the notch tip, that is far from the beam edges.

Different laws and theories have been derived to understand size effect such as statistical ones [8], fractal ones [9] or energetic ones [10, 11]. These have been confronted to several experimental results and two main laws can be highlighted. For type I, that is unnotched structures, we find in [12, 13]

$$\sigma_{\mathrm{N}} = f_r^{\infty}\left[1+\frac{rD_b}{D+l_p}\right]^{\frac{1}{r}} \tag{1}$$

where D_b is the effective thickness of the boundary layer, l_p is the effective width of the fracture process zone and r is a dimensionless parameter. σ_{N} denotes characteristic stress at failure, D a characteristic length of

*Corresponding author

the structure and Concerning type II size effect, that is for notched beams,

$$\sigma_{\mathrm{N}} = \frac{B f_t'}{\sqrt{1 + D/D_0}} \tag{2}$$

is given in [10] where f_t', D_0 and B are constants. Trying to find a unique universal law that could apply to both size effect types leads to different versions of similar laws. For example, in [14] the following law is given.

$$\sigma_{\mathrm{N}} = \left(1 + \frac{E' G_f}{g_0 D + (1-\lambda) c_f g_0' + \lambda E' G_f / {f_r^\infty}^2}\right)^{\frac{1}{2}} \left[1 + \frac{r \lambda D_b}{\sqrt{\bar{D} + l_p}}\right]^{\frac{1}{r}} \tag{3}$$

with

$$\lambda = \exp^{\alpha_0^k \left(\left[(\bar{D}/d_a)^p / q \right] \right.} \tag{4}$$

To summerize, G_f, c_f, f_r^∞, D_b, r, p, q, l_p and l_s are parameters to be determined, α_0 is the relative initial notch depth, d_a is the aggregate size, g is the dimensionless energy release rate function from LEFM and $\bar{D}$ is close to the beam depth which exact definition can be found in [14]. As size and shape models remain difficult to model, it has been preferred here to directly compare simulations and experimental data.

2. Thick level set model

We consider a material with the following free energy density [6]

$$\Phi(\varepsilon, d) = \mu(1 - \alpha_i d)\varepsilon_i^2 + \frac{\lambda}{2}(1 - \alpha d)\mathrm{tr}(\varepsilon)^2 \tag{5}$$

depending on strain ε and local damage d and where λ and μ are the Lamé elasticity coefficients, ε_i the eigenvalues of the strain tensor and

$$\left\{ \begin{array}{rlll} \alpha_i & = 0 & \text{if} & \varepsilon_i < 0 \\ & = 1 & \text{if} & \varepsilon_i \geq 0 \\ \alpha & = 0 & \text{if} & \mathrm{tr}(\varepsilon) < 0 \\ & = 1 & \text{if} & \mathrm{tr}(\varepsilon) \geq 0 \end{array} \right. \tag{6}$$

The potential is dissymmetric in tension and compression. If α and α_i were always equal to 1, the potential reduces to

$$\Phi(\varepsilon, d) = \frac{1}{2}(1 - d)\varepsilon : \mathbb{C} : \varepsilon \tag{7}$$

The stress σ and the local energy release rate Y are derived:

$$\sigma = \frac{\partial \Phi}{\partial \varepsilon}(\varepsilon, d) \quad \text{and} \quad Y = -\frac{\partial \Phi}{\partial d}(\varepsilon, d) \tag{8}$$

Let us consider a time-independent local damage model:

$$\left\{ \begin{array}{l} Y - h(d) Y_c \leq 0 \\ \dot{d} \geq 0 \\ (Y - h(d) Y_c)\dot{d} = 0 \end{array} \right. \tag{9}$$

The local critical energy release rate $h(d)Y_c$ depends on damage through the dimensionless function h, that is chosen to be 1 for $d = 0$ and monotonously increasing. The choice of the softening function h drives the form of the local stress-strain curve. As local damage models present spurious localization, some regularization is required. The thick level set damage model [15, 16, 17, 6] is one of them. The main idea of the thick level set damage model is to consider a damage front that drives damage evolution over a non local damage zone. The damage front is defined by the iso-zero of a signed-distance level-set function ϕ and damage only

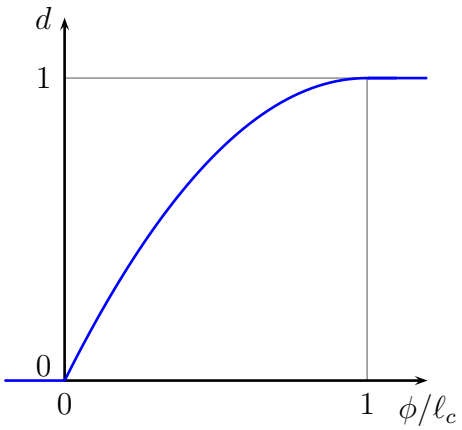

Figure 1: TLS classical damage profile.

depends on the local value of the level-set and a length parameter denoted ℓ_c. An example of damage profile $d(\phi/\ell_c)$ is given in Figure 1. Let us consider all the points of the damage band which have the same closest point to the damage front. Damage evolution of all those points is linked. So, a global criterion for all those points must be considered. It is chosen to replace Y and $h(d)Y_c$ in the local law (9) by averaged values denoted $\overline{Y}$ and $\overline{h(d)Y_c}$ defined by

$$\overline{Y} = \frac{\int_{\phi=0}^{\ell} Y d'(\phi) \left(1 - \frac{\phi}{\rho(s)}\right) \mathrm{d}\phi}{\int_{\phi=0}^{\ell} d'(\phi) \left(1 - \frac{\phi}{\rho(s)}\right) \mathrm{d}\phi} \quad \text{and} \quad \overline{h(d)Y_c} = Y_c \frac{\int_{\phi=0}^{\ell} h(d) d'(\phi) \left(1 - \frac{\phi}{\rho(s)}\right) \mathrm{d}\phi}{\int_{\phi=0}^{\ell} d'(\phi) \left(1 - \frac{\phi}{\rho(s)}\right) \mathrm{d}\phi} \tag{10}$$

where (s, ϕ) is a local basis, s a curvilinear abscissa of the front and $\rho(s)$ the curvature of the damage front. Note that the integrals are computed over a length depending on the width of the damaged band. So ℓ is increasing from 0 at initiation to ℓ_c when a totally damaged zone appears. At initiation, $\overline{h(d)Y_c} = h(0)Y_c = Y_c$ and $\overline{Y}$ is equal to its local value. The evolution law then becomes

$$\begin{cases} \overline{Y} - \overline{h(d)Y_c} \leq 0 \\ \dot{\phi} > 0 \\ (\overline{Y} - \overline{h(d)Y_c})\dot{\phi} = 0 \end{cases} \tag{11}$$

On the choice of the softening function $h(d)$. The simplest softening function is the constant one $h(d) = 1$. It leads to a perfectly brittle behavior. An interesting softening function is presented in [18] from a comparison between the cohesive model and TLS. It is shown that it is possible to derive a one-dimensional TLS local behavior from some classical cohesive laws. In particular, for a given bi-linear cohesive law (see Figure 2) and for a large range of TLS characteristic length ℓ_c, a softening function $h(d)$ is explicitly derived in order to have the same macroscopic behavior for a one-dimensional bar. Using this softening function in bi-dimensional problems leads to very satisfactory results as local and global behaviors are close to cohesive model ones [18]. In this paper, we will only consider this kind of CZM-like softening functions. Note that in equations (37), (45), (49), (50) and (63) from [18] the integration variable should be d and not $\tilde{phi}$. An example of such a local stress-strain curve is given in Figure 3. Let us note that the behavior curves so obtained present a discontinuity that appears as a linear zone where strain and stress increase while damage remains constant. Its origin is the slope discontinuity on the cohesive behavior.

3. Calibration of the parameters

In order to identify experimental results concerning size and geometry effects, a general method has been established to calibrate the parameters of the model that can be splitted into two categories: those coming

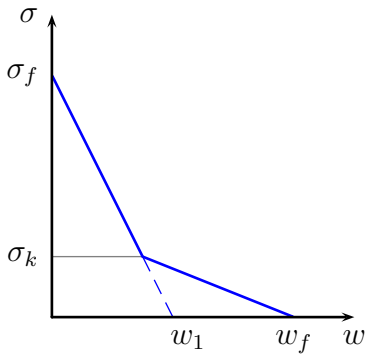

Figure 2: Bilinear cohesive behavior

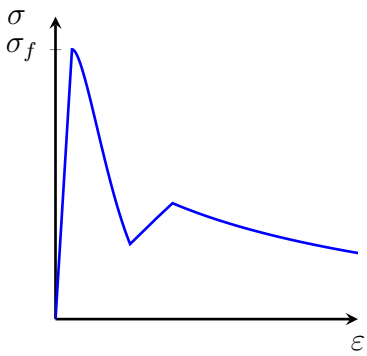

Figure 3: Example of a local softening behavior obtained by a one-dimensional comparison between TLS and cohesive models and corresponding to a bi-linear cohesive behavior [18].

from TLS regularization and those defining the local behavior. The last ones are in fact chosen to be the cohesive parameters of a bilinear tension-opening curve as explained in [18].

3.1. CZM parameters

Four scalar values describe the bilinear cohesive behavior: σ_f, σ_k, w_1 and w_f (see Figure 2). From them, we can derive two values of the LEFM critical energy release rate [19]. The first one here denoted G_f comes from a size effect analysis [20]; the second one, G_F, corresponds to the total amount of energy needed to break a beam [21].

$$G_f = \frac{1}{2}\sigma_f w_1, \qquad G_F = G_f + \frac{1}{2}\sigma_k(w_f - w_1) \tag{12}$$

Moreover, σ_f is linked to the tensile strength of a splitting test f_t. In calibrating the model, these three measurable quantities are considered as initial values. A degree of freedom remains. It is arbitrarily fixed by $\sigma_k = \frac{\sigma_f}{2}$. Thus

$$\sigma_f = f_t, \quad w_1 = \frac{2G_f}{\sigma_f}, \quad \sigma_k = \frac{\sigma_f}{2} \quad \text{and} \quad w_f = \frac{2(G_F - G_f)}{\sigma_k} + w_1 \tag{13}$$

These values are a starting point to calibrate the parameters. After running a simulation with this set of parameters, it is then recommended to modify them in function of the results obtained. First, σ_f should be modified in order to fit the maximum load of the larger unnotched beam (from eq. (1), the peak stress σ_f should be recovered for infinitely large beams). Next, w_1 has to be modified to fit the maximum load of the

larger notched beam containing the deeper initial notch in the spirit of type II size-effect. The form of the force-opening curve around the peak can also be considered. Finally, σ_k and w_f can be slightly adapted to fit the post-peak results. It is important to note that some conditions apply on the choice of the cohesive parameters [18]. They correspond to the mathematical condition to have an increasing local energy release rate Y with respect to damage d.

3.2. TLS parameters

Two parameters come from TLS regularization: the characteristic length ℓ_c and the damage profile $d(\phi/\ell_c)$. These parameters are chosen to be close to FPZ characteristics such as its width and damage distribution. In [4], lattice simulations of three point bending concrete beams under centered loading were performed. In [22], it is shown that both experimental and numerical results are similar for the width of the damaged band. Its size is between 10 mm (energetic analysis) and 40 mm (damage analysis), depending on which quantities are actually studied. In [23], it is shown by using Ripley's functions to extract correlation length between damage points in lattice simulations that correlation length is about 50 mm. This analysis gives the order of magnitude of FPZ width but not a precise value. Thus, numerical considerations are taken into account. The bi-dimensional comparison between cohesive and TLS models showed that better agreement corresponds to smaller values of ℓ_c. It is then chosen here to keep $\ell_c = 20$ mm that corresponds to 40 mm-wide fracture process zone. However, this implies to neglect a part of the damage that is more diffuse than the concentrated one around the crack (see Figure 4).

The damage profile is mainly identified from the damage distribution obtained in lattice simulations. In order to be able to compare localized damage interface values of lattice model with the continuum damage values of the TLS, an averaging method has been applied to lattice results. Let us denote x the horizontal coordinate (0 is centered) and y the vertical one (origin is at notched edge) as in [22]. The notch's coordinates are $(x = 0, 0 < y < y^{\text{notch}}_{\text{max}})$. The damage profile is analyzed over a band $y \in [10\text{mm}, 16\text{mm}]$ in the specimen $(n = 2, i = 1)$, that is slightly ahead initial notch, in order to avoid boundary phenomena and to analyze a profile that is close enough to a self-similar propagation of a crack. Over that band, averaged values of interface damage are computed with a uniform weight over zones of 10 mm width. Results are shown in 4. The chosen damage profile, an inverted parabola (see Figure **??**) is also drawn. Both are close where damage is concentrated but differ when damage is more diffuse. In fact, it is chosen here to neglect this diffuse damage. Note that an improved version of the TLS [24] is able to take into account both diffuse and localized damage zones.

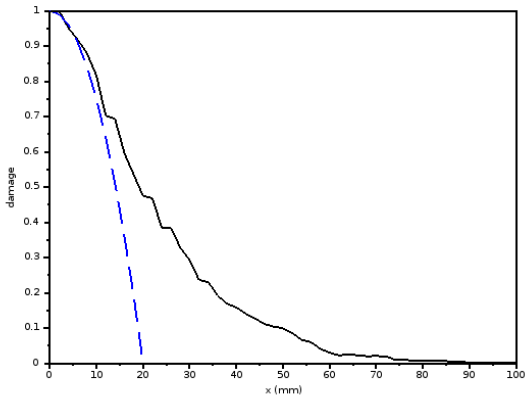

Figure 4: Averaged interface damage from lattice simulations (plain, black) and identified damage profile for pure non local TLS regularization (dashed, blue).

4. Fit to experimental data

Two main experimental campaigns [2, 3] on concrete three point bending beams of different sizes and notch depths are considered in this paper. They present a particular interest as both size and shape effects are tested on the same material and conditions. Moreover, the results have already been fitted by other methods (cohesive crack for Hoover *et al.*experimental data [3] as shown in [5] on the one hand and integral nonlocal [2] and lattice model [4] for Grégoire *et al.*experimental data [2]). These fits have shown the capability of the cohesive crack and the lattice meso-scale models to properly reproduce size and shape effects. They also brought out the difficulty of the integral nonlocal regularization to accurately simulate both effects and was later confirmed by [25]. So, from three different families of models (cracks, damage and lattice ones) only two seem to be able to describe size and shape effects.

Both campaigns concern three point bending tests performed on single edge notched beams or unnotched ones. The load and the notch, when it exists, are always centered. The various beams for each campaign and notch depth are geometrically similar in 2D and the same thickness is kept. Both concrete formulations include similar largest aggregate sizes: maximum diameter is 10 mm for [3] and are between 10 mm and 14 mm for [2]. Let us remark that a different method is used to create the notch: in [3], it is sawed (1.5 mm width) and in [2] it is molded (2 mm width). More details on the experimental protocols are given in [2, 3].

All simulations are performed with similar numerical parameters: the mesh density is kept constant over the damaged zone (about $\frac{\ell_c}{20}$). The maximum front advance at each step is between 0.25 and 0.7 times the characteristic size of the mesh. The value is set close to 0.7 for larger specimen and close to 0.25 for smaller ones.

4.1. Comparison with Grégoire et al. experiments

Four beam sizes are considered (400 mm, 200 mm, 100 mm and 50 mm depth) and three notch relative depth (0, 0.2 and 0.5) as described in Figure 5. The span-to-depth ratio is 2.5. Geometries are described by two integers: n for the size (1 is the larger and 4 the smaller) and i for the notch depth (1 for half-notched, 2 for fifth-notched and 3 for unnotched). Parameters given in Table 1 correspond to the best fit obtained by the authors, shown in Figures 6.

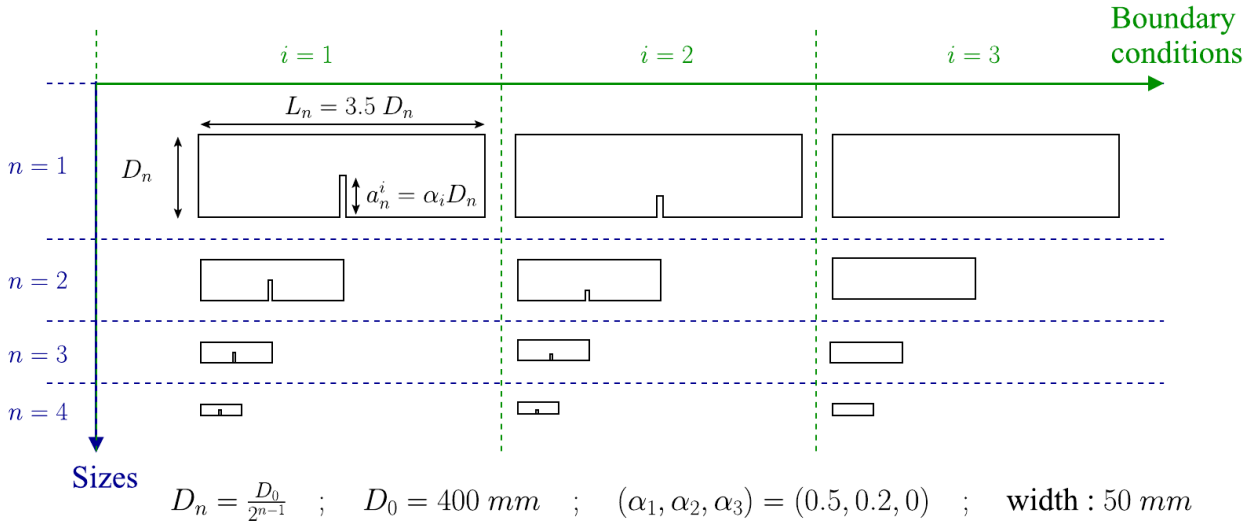

Figure 5: Description of beam geometries (from [2])

Results show good agreement between experimental data and TLS simulations. The main force-opening response is well reproduced even if some differences exist, in particular for the specimens $(n = 1, i = 2)$ and $(n = 1, i = 3)$. However it is worth mentioning that the lattice model does not fit the $(n = 1, i = 2)$ curve and no results are furnished in [4] for the late post-peak response of the $(n = 1, i = 3)$ case.

	TLS simulation parameters
σ_f	3.8 MPa
σ_k	1.8 MPa
w_1	23 μm
w_f	55 μm

Table 1: Cohesive law values of the best fit obtained by authors for Grégoire *et al.* experimental campaign [2]

	cohesive simulations [5]	TLS simulations
σ_f	3.92 MPa	4.2 MPa
σ_k	0.588 MPa	1.5 MPa
w_1	25.3 μm	23.5 μm
w_f	94.8 μm	40 μm

Table 2: Cohesive law values of the best fit obtained by authors for Hoover *et al.* experimental campaign and parameters used in [3]

.

It is important to note that for $(n = 1, i = 2)$ and $(n = 1, i = 3)$ simulated curves, a jump can be observed in the force-opening curve. Its existence is strongly linked to the maximal front advance per step, that is driven by a purely numerical coefficient. Even if some implementation effort must be done to avoid this, the artifact should not contest the physical meaning of TLS results.

4.2. Comparison with Hoover et al. experiments

Four beam sizes are considered (500 mm, 215 mm, 93 mm and 40 mm depth) and five notch relative depth (0, 0.025, 0.075, 0.15 and 0.3). For relative depth 0.025, only the two biggest beams (500 mm and 215 mm) were tested in the experimental campaign. The span-to-depth ratio is 2.176. The geometries are described by two letters: a capital one for the size ("A" is the larger and "D" the smaller) and a lowercase one for the notch depth ("a" for 0.3-notched and "e" for unnotched). Parameters given in Table 2 correspond to the best fit obtained by the authors, shown in Figures 7 and 8. Let us remark that the best fit obtained by the authors corresponded to parameters slightly different from those used in cohesive simulations of [5]. Nevertheless, the main parameters that drive load peak values, σ_f and w_1, are very close.

Very good accuracy between experimental data and TLS simulations is observed: both maximum load and force-opening curves are well recovered. The quality of TLS fit is similar to cohesive one even if the cohesive behavior parameters are not exactly the same. Let us remind that cohesive and TLS damage models theoretically coincide for ℓ_c infinitely close to zero [18]. As ℓ_c is not zero in practice, behaviors are slightly different which explains the differences between pure CZM parameters and the set of CZM-like parameters used in TLS simulations. Comparing The quality of this fit is better than the previous one (see section 4.1). This could be explained by the difference in the way the notch was done. Hoover *et al.*sawed it while Grégoire *et al.*molded them. The structure and properties of concrete around the notch tip can the be modified due to autogenous shrinkage during concrete curing for a molded notch. Furthermore, aggregates distribution around the notch tip is diferent in both cases: large aggregates has a lower probability to be close to the boundary than smaller ones. So, molded notchs have a modified aggregates distribution compared to sawed ones.

5. Conclusions and perspectives

It has been shown that the TLS damage regularization is able to recover size and shape effects. Its accuracy is close to cohesive zone and lattice models ones. To the authors knowledge, no continuum damage model has been able to provide similar results so far.

The one dimensional comparison analytically established between the cohesive model and the TLS regularization in [18] furnished a pertinent local behavior. Nevertheless, two main issues to improve the results

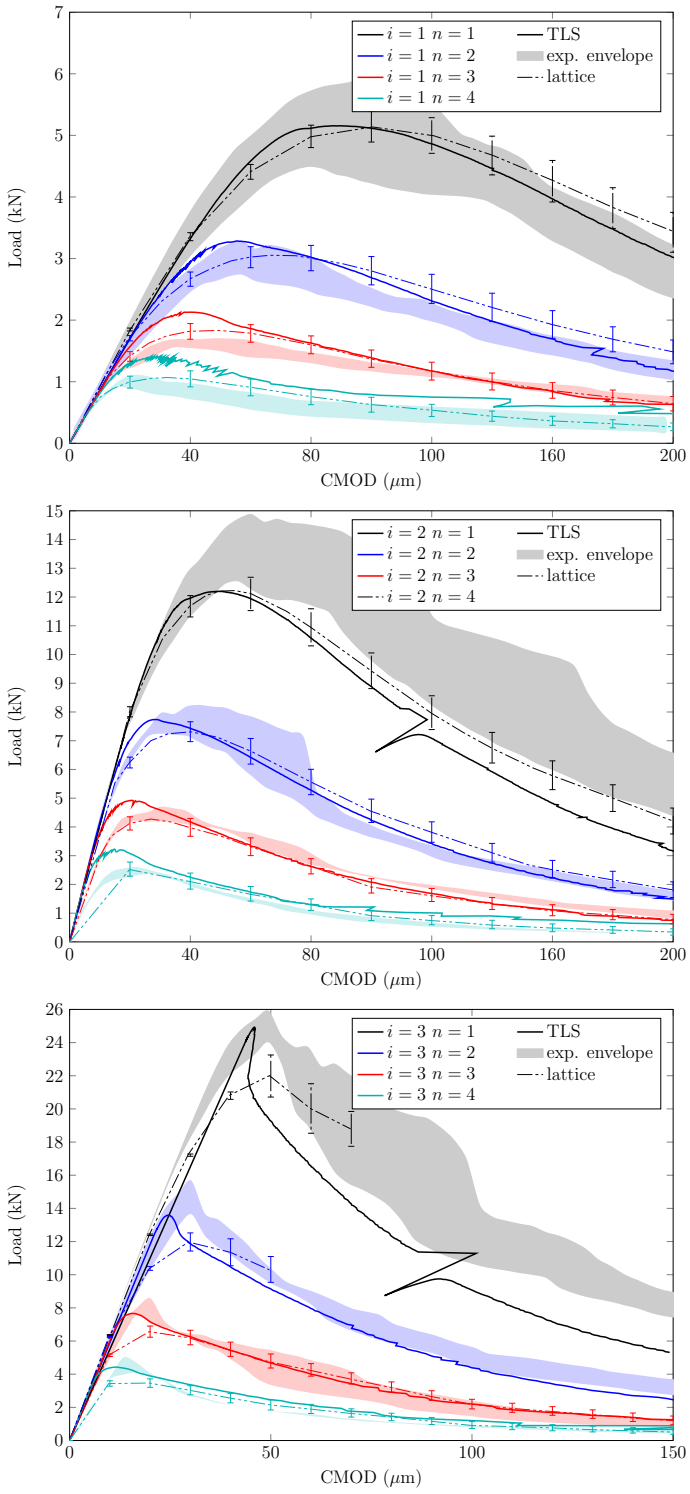

Figure 6: Comparison between TLS simulations, lattice ones [4] and experimental data [2]. Raw data is drawn for TLS simulations.

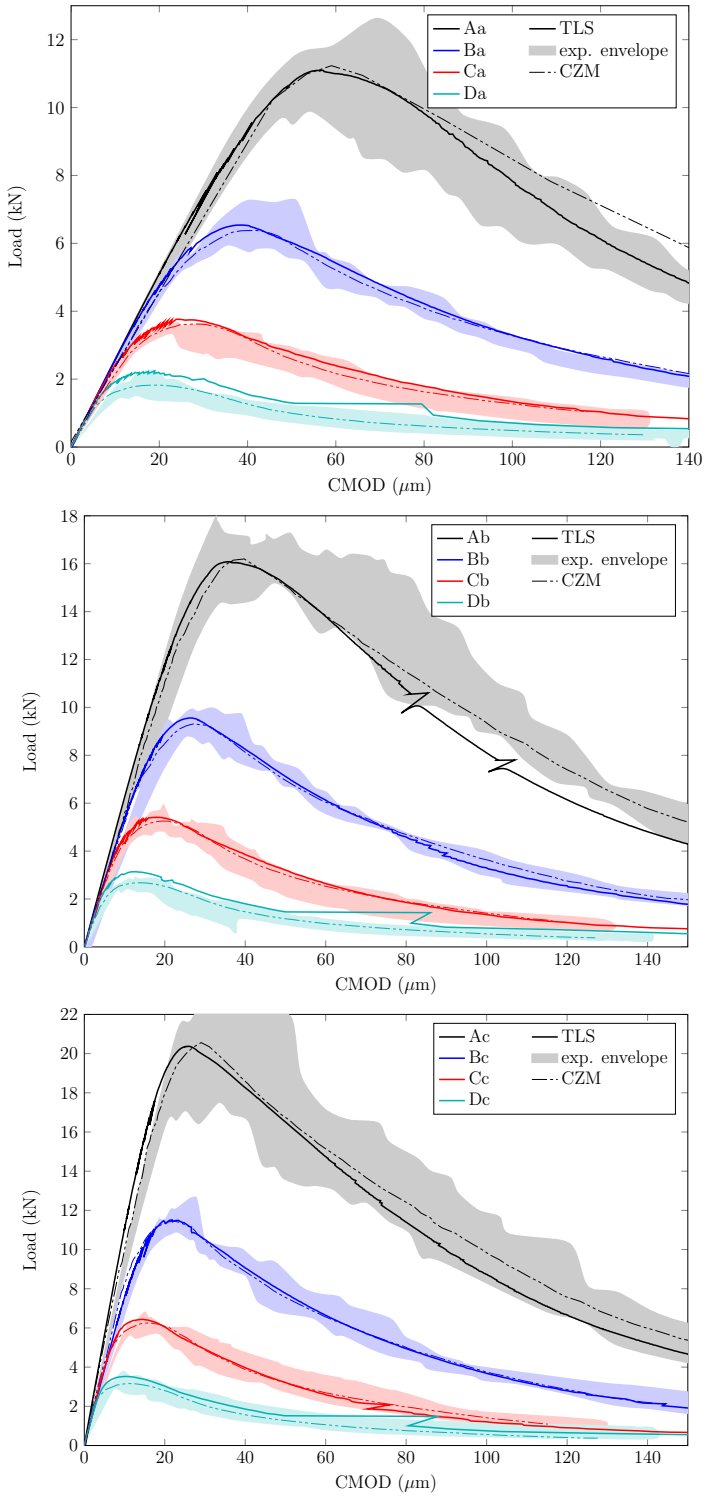

Figure 7: Comparison between TLS simulations, lattice ones [4] and experimental data [2]. Raw data is drawn for TLS simulations.

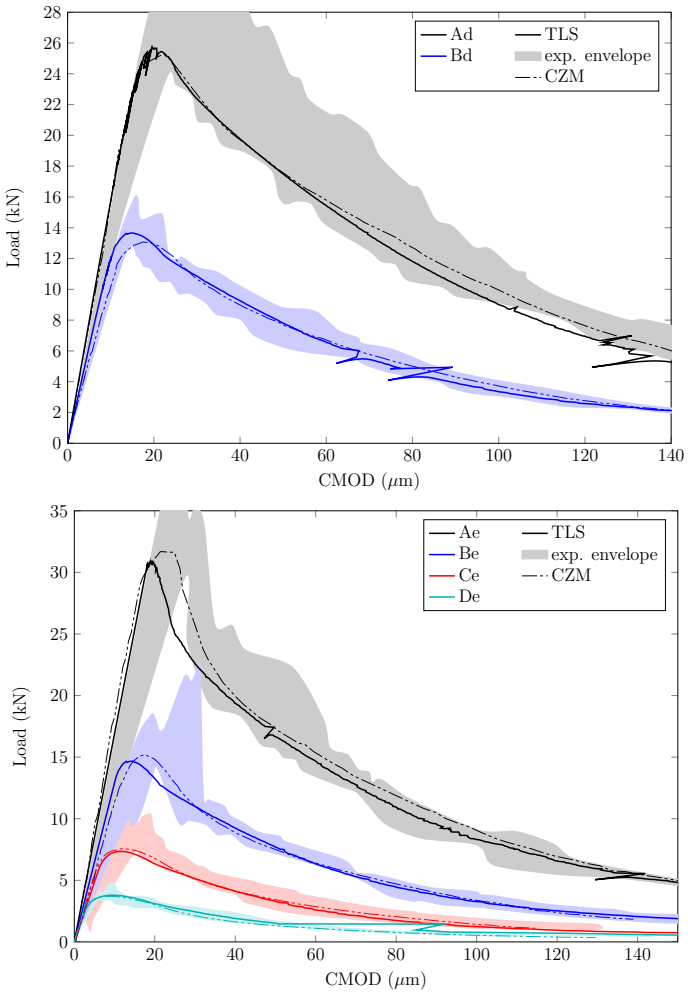

Figure 8: Comparison between TLS simulations, lattice ones [4] and experimental data [2] (continuation). Raw data is drawn for TLS simulations.

arise. First, the CZM-like behavior obtained is not smooth. This could explain some spurious oscillations observed on TLS simulated results. It could be useful to look for a similar softening function presenting better regularity properties. Second, as it has been explained previously, the TLS version used in this paper only deals with localized damaged while diffuse damage is observable in experimental tests [26, 27]. Theoretical developments and associated implementations are already being performed to improve the model in that sense. This should give better results for smaller specimen simulations.

6. Bibliography

References

[1] Z. P. Bažant, "Size effect on structural strength: a review," *Archive of Applied Mechanics (Ingenieur Archiv)*, vol. 69, pp. 703–725, Nov. 1999.

[2] D. Grégoire, L. Rojas-Solano, and G. Pijaudier-Cabot, "Failure and size effect for notched and unnotched concrete beams," *International Journal for Numerical and Analytical Methods in Geomechanics*, vol. 37, pp. 1434–1452, July 2013.

[3] C. G. Hoover, Z. P Bažant, J. Vorel, R. Wendner, and M. H. Hubler, "Comprehensive concrete fracture tests: Description and results," *Engineering Fracture Mechanics*, vol. 114, pp. 92–103, 2013.

[4] P. Grassl, D. Grégoire, B. Rojas-Solano, Laura, and G. Pijaudier-Cabot, "Meso-scale modelling of the size effect on the fracture process zone of concrete," *International Journal of Solids and Structures*, vol. 49, pp. 1818–1827, June 2012.
[5] C. G. Hoover and Z. P. Bažant, "Cohesive crack, size effect, crack band and work-of-fracture models compared to comprehensive concrete fracture tests," *International Journal of Fracture*, vol. 187, no. 1, pp. 133–143, 2014.
[6] N. Moës, C. Stolz, P.-E. Bernard, and N. Chevaugeon, "A level set based model for damage growth: The thick level set approach," *International Journal for Numerical Methods in Engineering*, vol. 86, pp. 358–380, Apr. 2011.
[7] P. F. Walsh, "Fracture of plain concrete," *Indian Concrete Journal*, vol. 46, no. 11, 1972.
[8] W. Weibull, *The phenomenon of rupture in solids*. Generalstabens Litografiska Anst., 1939.
[9] A. Carpinteri, "Fractal nature of material microstructure and size effects on apparent mechanical properties," *Mechanics of Materials*, vol. 18, no. 2, pp. 89–101, 1994.
[10] Z. P. Bažant, "Size effect in blunt fracture: concrete, rock, metal," *Journal of Engineering Mechanics*, vol. 110, no. 4, pp. 518–535, 1984.
[11] Z. P. Bažant and J. Planas, *Fracture and Size Effect in Concrete and Other Quasibrittle Materials*. CRC Press, 1998.
[12] Z. P. Bažant, "Scaling of quasibrittle fracture: asymptotic analysis," *International Journal of Fracture*, vol. 83, no. 1, pp. 19–40, 1997.
[13] Z. P. Bažant and Q. Yu, "Universal size effect law and effect of crack depth on quasi-brittle structure strength," *Journal of engineering mechanics*, vol. 135, no. 2, pp. 78–84, 2009.
[14] C. G. Hoover and Z. P. Bažant, "Universal size-shape effect law based on comprehensive concrete fracture tests," *Journal of Engineering Mechanics*, vol. 140, no. 3, pp. 473–479, 2014.
[15] P. Bernard, N. Moës, and N. Chevaugeon, "Damage growth modeling using the Thick Level Set (TLS) approach: Efficient discretization for quasi-static loadings," *Computer Methods in Applied Mechanics and Engineering*, vol. 233-236, pp. 11–27, Aug. 2012.
[16] C. Stolz and N. Moës, "A new model of damage: a moving thick layer approach," *International journal of fracture*, vol. 174, no. 1, pp. 49–60, 2012.
[17] C. Stolz and N. Moes, "On the rate boundary value problem for damage modelization by thick level-set," *ACOMME-2012*, pp. 205–220, 2012.
[18] A. Parrilla Gómez, N. Moës, and C. Stolz, "Comparison between Thick Level Set (TLS) and cohesive zone models," 2015.
[19] Z. P. Bažant, "Size effect aspects of measurement of fracture characteristics of quasibrittle material," *Advanced Cement Based Materials*, vol. 4, no. 3, pp. 128–137, 1996.
[20] Z. P. Bazant and P. A. Pfeiffer, "Determination of fracture energy from size effect and brittleness number," *ACI Materials Journal*, vol. 84, no. 6, 1987.
[21] RILEM, "Determination of the Fracture Energy of Mortar and Concrete by Means of Three-Point Bend Tests on Notched Beames," *Materials and Structures*, vol. 18, no. 106, pp. 285–290, 1985.
[22] D. Grégoire, L. Verdon, V. Lefort, P. Grassl, J. Saliba, J.-P. Regoin, A. Loukili, and G. Pijaudier-Cabot, "Mesoscale analysis of failure in quasi-brittle materials: comparison between lattice model and acoustic emission data," *International Journal for Numerical and Analytical Methods in Geomechanics*, 2015.
[23] V. Lefort, G. Pijaudier-Cabot, and D. Grégoire, "Analysis by ripley's function of the correlations involved during failure in quasi-brittle materials: Experimental and numerical investigations at the mesoscale," *Engineering Fracture Mechanics*, vol. 147, pp. 449–467, 2015.
[24] N. Moës, C. Stolz, and N. Chevaugeon, "Coupling local and non-local damage evolutions with the Thick Level Set model," *Advanced Modeling and Simulation in Engineering Sciences*, vol. 1, no. 1, pp. 1–21, 2014.
[25] S. Y. Alam, P. Kotronis, and A. Loukili, "Crack propagation and size effect in concrete using a non-local damage model," *Engineering Fracture Mechanics*, vol. 109, pp. 246–261, 2013.
[26] K. Haidar, G. Pijaudier-Cabot, J. F. Dubé, and A. Loukili, "Correlation between the internal length, the fracture process zone and size effect in model materials," *Materials and Structures*, vol. 38, pp. 201–210, Mar. 2005.
[27] S. Y. Alam, J. Saliba, and A. Loukili, "Study of evolution of fracture process zone in concrete by simultaneous application of digital image correlation and acoustic emission," 2013.